



Enhanced adsorption of uranium (VI) using a three-dimensional layered double hydroxide/graphene hybrid material

Lichao Tan^a, Yulan Wang^b, Qi Liu^{a,*}, Jun Wang^{a,c,*}, Xiaoyan Jing^a, Lianhe Liu^c, Jingyuan Liu^a, Dalei Song^a

^a Key Laboratory of Superlight Material and Surface Technology, Ministry of Education, Harbin Engineering University, Harbin 150001, China

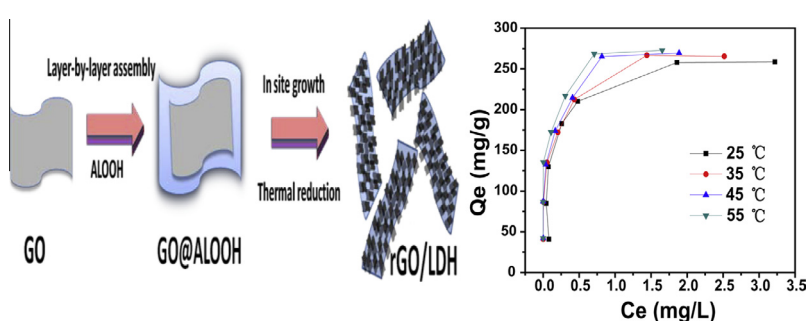
^b Inner Mongolia Vocational College of Chemical Engineering, Hohhot 010010, China

^c Institute of Advanced Marine Materials, Harbin Engineering University, 150001, China

HIGHLIGHTS

- A hierarchical three-dimensional composite (rGO/LDH) was prepared and well characterized.
- Uranium (VI) removal using rGO/LDH was studied for the first time.
- The adsorption process for uranium (VI) removal was studied in detail.
- rGO/LDH exhibited fast and efficient sorption for uranium (VI).

GRAPHICAL ABSTRACT



ARTICLE INFO

Article history:

Received 18 June 2014

Received in revised form 5 August 2014

Accepted 6 August 2014

Available online 15 August 2014

Keywords:

Uranium (VI)

Graphene

Layered double hydroxides

Adsorption

ABSTRACT

This study presents a facile route for the fabrication of a hierarchical three-dimensional composite (layered double hydroxide/graphene). The composite was obtained via in situ growth of layered double hydroxide (LDH) nanosheet arrays onto graphene sheets. The materials were characterized by transmission electron microscopy, scanning electron microscope, Fourier-transform infrared spectroscopy, X-ray diffraction and Brunauer–Emmett–Teller surface area measurement. This particularly structured composite has a large specific surface area and typical mesoporous characteristics, which are favorable for achieving high adsorption performance. The influence of conditions for uranium adsorption, including pH of aqueous solution, adsorbent dose, shaking time, and temperature were investigated. The results reveal that the maximum adsorption capacity of the layered double hydroxide/graphene toward uranium (VI) is 277.80 mg g⁻¹, displaying a high efficiency for the removal of uranium (VI) from aqueous solution. The thermodynamic parameters, such as ΔH° , ΔS° , and ΔG° show that the process is endothermic and spontaneous. The kinetic adsorption can be described by a pseudo-second-order rate equation. This work describes an efficient, fast, and convenient approach for the removal of uranium (VI) from aqueous solutions.

© 2014 Elsevier B.V. All rights reserved.

1. Introduction

The shortage of economical, sustainable, low-carbon energy sources is an inevitable problem facing humanity. Nuclear energy as an economical and clean energy source for sustainable development has been widely developed to provide base-load

* Corresponding authors. Address: Key Laboratory of Superlight Material and Surface Technology, Ministry of Education, Harbin Engineering University, Harbin 150001, China (J. Wang). Tel./fax: +86 451 8253 3026.

E-mail address: zhqw1888@sohu.com (J. Wang).

power, currently comprising 13.8% of global energy production [1]. Therefore, reasonable and effective development of nuclear energy can fundamentally change the world energy structure [2–4]. Uranium is an element of considerable interest due to its importance for energy and weapons industries. It is estimated that sufficient uranium remains for 70 years of nuclear power generation if the current rate of consumption is maintained [5], making the extraction and recovery of uranium (VI) from unconventional sources essential for long-term resource availability. Up to date, many technologies to treat uranium (VI) containing aqueous solutions have been developed, including chemical precipitation, organic and inorganic ion exchange, physical and chemical adsorption, electrodialysis, and solvent extraction process [6–9]. More notably, adsorption seems to be one of the most effective methods owing to its economical, cost-effective and simple features in removing trace levels of ions [10–13].

Different types of adsorbents have been tested for recovery of uranium (VI) from aqueous media. Among them, graphene has recently attracted great attention due to its remarkable properties, such as huge surface area (with a calculated value of $2630 \text{ m}^2 \text{ g}^{-1}$), good chemical stability, and graphitized basal plane structure [14,15]. Therefore, graphene has become an attractive candidate as a novel nanoscale building block for adsorption of uranium (VI) from aqueous solutions [16]. However, to the best of our knowledge, graphene is hydrophobic and usually suffers from irreversible agglomeration in water due to the strong van der Waals interactions between neighboring sheets, which leads to a great loss of effective surface area and consequently a lower adsorption capacity than expected [17,18]. To prevent the restacking of graphene nanosheets, many studies have recently focused on the intercalation of inorganic nanoparticles (MnO_2 [19], Co_3O_4 [20] and $\text{Ni}(\text{OH})_2$ [21]), into graphene interlayers.

In the past few years, layered double hydroxides (LDHs) containing transition metals have been employed as adsorption materials. LDHs have the structural formula: $[\text{M}_1^{2+}{}_{1-x}\text{M}_2^{3+}{}_x(\text{OH})_2]^{x+}[\text{A}^{n-}]_{x/n} \cdot m\text{H}_2\text{O}$, in which M_1^{2+} and M_2^{3+} are divalent and trivalent metal cations, and A^{n-} is an interlayer anion. Their large interlayer space and high concentration of active sites have allowed for a series of multifunctional LDH materials to be used as anion exchangers [22], absorbents [23,24], and magnetic materials [25,26]. However, for almost all of the reported LDHs, the LDH nanosheets parallel piled up together and are far from orderly and uniform. As a result, the specific areas of LDHs are relatively low leading to low adsorption capacity.

Taking the aforementioned factors into account for our study, a 3D hierarchical composite with graphene sandwiched between two layers of NiAl-LDH nanosheets has been synthesized using a simple and cost effective in situ growth procedure. As an adsorbent for uranium (VI), several advantages of this adsorbent make it especially attractive. First, it is fabricated using a facile, non-toxic synthetic route. Second, the larger specific surface area of the composite can provide more adsorptive sites. Third, it can be used for effective adsorption/recovery of uranium (VI) ions. The combined properties of rGO/NiAl-LDH hold great promise in a wide range of fields.

2. Experimental

2.1. Preparation of samples

The graphene oxide (GO) was obtained according to the previous report [27]. Using an ultrasonication method exfoliated GO, 1 mg mL^{-1} GO aqueous suspension was prepared by dispersing the graphene oxide in deionized water. Based on the AlOOH product coating onto the surface of GO, the rGO/NiAl-LDH composite

was prepared by an in situ growth procedure; the precursor was denoted as the GO@AlOOH composite. First, the boehmite AlOOH primer sol was obtained by hydrolysing aluminum isopropoxide according to a previous report [28]. Using a layer-by-layer (LBL) technique we prepared the GO@AlOOH composite. Typically, 20 mL of the as-obtained AlOOH sol was mixed with a 6 mL GO solution using vigorous agitation for 12 h. Subsequently, the sample was separated by centrifugation, rinsed with ethanol several times and then dried at room temperature.

A sandwich-structured composite was formed according to an in situ crystallization process in which NiAl-LDH nanosheets grew on the surface of the GO@AlOOH sheets. In a typical procedure, the brown GO@AlOOH powder was homogeneously dispersed in 30 mL of deionized water by ultrasonication and vigorous stirring. 0.3 g of urea and 3 mL of $\text{Ni}(\text{NO}_3)_2$ (0.5 mol L^{-1}) were then added into the above solution. After stirring for 20 min, the mixed solution was placed in an autoclave and heated at 120°C for 24 h. The resulting product is denoted as rGO/NiAl-LDH. The whole fabrication and growth process of the composite is depicted in Fig. 1.

2.2. Characterization

X-ray diffraction (XRD) analysis was performed on a Rigaku D/max-IIIB diffractometer with $\text{CuK}\alpha$ irradiation ($K\alpha = 1.54178 \text{ \AA}$). The X-ray source was operated at 40 kV and the current used in XRD measurements is 150 mA. Fourier-transform infrared (FT-IR) spectrum was recorded with an AVATAR 360 FT-IR spectrophotometer using standard KBr pellets. N_2 adsorption/desorption isotherms were measured at liquid nitrogen temperature (-196°C) using a Micromeritics ASAP 2010 instrument. The specific surface areas were calculated using the Brunauer–Emmett–Teller (BET) method. Pore size distributions were calculated from the adsorption branch of the N_2 adsorption/desorption isotherms using the Barret–Joyner–Halenda (BJH) method. The morphologies of the samples were characterized using a transmission electron microscope (TEM, FEI Tecnai G2 S-Twin) and a scanning electron microscope (SEM, JSM-6480A, Japan Electronics), equipped with an energy dispersive X-ray spectrometry analyzer (EDS, INC250, Japan Electronic).

2.3. Adsorption experiments

The effects of solution pH, contact time, initial concentrations and temperature on adsorption of uranium (VI) were investigated. Typically, an amount of the adsorbent (0.01 g) was added into 20 mL uranium (VI) solution of given concentration and pH value in a conical flask. The pH was adjusted by 0.1 mol/L HNO_3 and NaOH solution. The mixture was shaken for 3 h in a thermostatic shaker bath. The suspension was centrifuged at 5000 rpm for 10 min at room temperature. The concentration of uranium (VI) in the solution was determined by Bruker 820-MS ICP-MS instrument. The adsorption capacity Q_e (mg g^{-1}) and the % removal of uranium were calculated according to Eqs. (1) and (2):

$$Q_e = \frac{(C_0 - C_e)V}{m} \quad (1)$$

$$\text{Removal (\%)} = \frac{100(C_0 - C_e)}{C_0} \quad (2)$$

where C_0 (mg L^{-1}) is the uranium (VI) ion concentration in the initial solution, C_e (mg L^{-1}) is the equilibrium concentration of uranium (VI) ion in the supernatant, V (L) is the volume of the testing solution and m is the weight of sorbent (g).

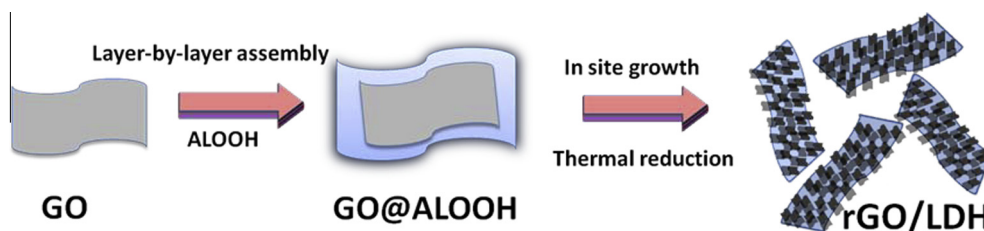


Fig. 1. Schematic illustration for the formation process of rGO/NiAl-LDH composite.

2.4. Desorption studies

To investigate the reusability of rGO/LDH, 0.01 g of rGO/LDH was first put in contact with 20 mL uranium (VI) for 120 min. After adsorption, desorption was carried out by washing the adsorbents with distilled water several times, and then the solution containing 20 mL of desorptive solutions was added into the adsorbed uranium (VI) adsorbents for 120 min. Before the second adsorption, the adsorbent was treated by $0.1 \text{ mol L}^{-1} \text{ NaHCO}_3$ solution for 120 min. The samples were separated from the solution by 5000 rpm centrifugation. The above procedure was repeated three times to test the reusability of the rGO/LDH.

3. Results and discussion

3.1. Characterization of samples

Fig. 2 shows the XRD patterns of as-synthesized rGO, GO, NiAl-LDH and rGO/NiAl-LDH, respectively. In the XRD pattern of GO (Fig. 2B), we can see a sharp diffraction peak at 10.8° , which is assigned to GO. The (001) interlayer spacing of the as-obtained exfoliated GO is calculated to be 0.82 nm, showing an complete oxidation of graphite to the graphite oxide due to the introduction of oxygen-containing functional groups on the graphite sheets [29]. After GO is reduced to rGO by glucose, the peak at 10.8° completely disappears and a broad peak corresponding to rGO at about 24.5° with an interlayer spacing of 0.36 nm is observed (Fig. 2A), which is still a little larger than that of natural graphite (0.34 nm). This is attributed to the π - π stacking interaction between the graphene sheets leading to the formation of the agglomerates. For pure NiAl-LDH (Fig. 2C), the XRD pattern is indexed to rhombohedral NiAl-LDH (JCPDS No. 15-0087) in a $R3m$ space group. The basal spacing (d_{003}) of the pure NiAl-LDH is about 0.76 nm, which is similar to that reported in other articles, indicating that CO_3^{2-} ions and water molecules have been intercalated into the interlayer spaces [30]. In the case of rGO/LDH

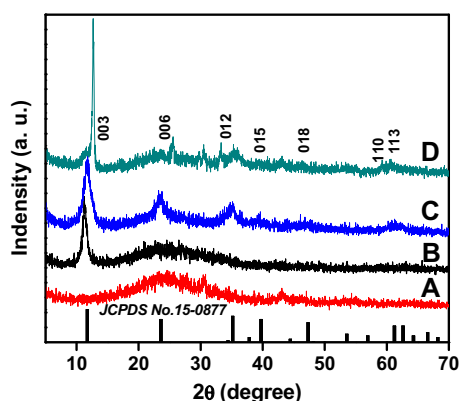


Fig. 2. Typical XRD patterns of rGO (A), the GO (B), Ni-Al LDH (C), and the prepared rGO/LDH composite (D).

(Fig. 2D), the peaks for the (003), (006), (012) and (015) planes are also in accordance with rhombohedral NiAl-LDH. The value of d_{003} is calculated to be 0.77 nm, which is a little wider than that of pure NiAl-LDH. This is ascribed to weakened electrostatic interactions between the brucite-like sheets and interlayer species, probably involving the driving force of NiAl-LDH grown onto the graphene surfaces [31,32]. Previous research also shows that if the regular stacks of graphite or graphite oxide are destroyed, the diffraction peaks will become weaker or even disappear [33–35]. However, the relatively weaker intensity of the peaks of rGO/LDH compared with those of pure NiAl-LDH means a low crystallinity of the hybrid material.

The microstructures of the products were further characterized by means of SEM and TEM measurements, as shown in Fig. 3. The SEM image of pure NiAl-LDH (Fig. 3A) shows that the product is composed of a number of inhomogeneous flakes, while most of the NiAl-LDH sheets stack with each other to form agglomerates. A closer observation of the rGO/LDH composite shows that the LDH nanosheet arrays are grown on both sides of the graphene sheets (highlighted by the red circle in Fig. 3B), efficiently avoiding the aggregation and stacking of individual graphene sheets and leading to an interesting 3D sandwich structure. In this three-layer-structure, the rGO sheets are located in the middle and are sandwiched between two LDH nanosheet layers. EDS analysis in Fig. 3C shows that the composite consists of C, O, Al and Ni elements, suggesting that graphene and NiAl-LDH co-exist in the composite. Such a 3D structure with a perpendicular growth of LDH nanosheet arrays on the surface of graphene is also confirmed from TEM images (Fig. 3D and E). As shown, the LDH nanosheets grow upright on the graphene substrate and are around 20 nm in thickness. Scrolling and corrugation can be clearly observed at the edge of the slice. Although there is little difference in the contrast between LDH nanosheets and the graphene substrate, it can be observed that the graphene sheets still exist in the sandwich structured composite from these well-known typical features. Therefore, a three-dimensional layered double hydroxide nanosheet array/graphene composite was prepared.

The physical properties of LDH and rGO/LDH are shown in Fig. 4. Both curves show typical IV isotherms with an H3-type hysteresis loop ($P/P_0 > 0.4$), demonstrating the existence of mesopores in both samples. The pore volume and surface area of the rGO/LDH composite are $0.66 \text{ cm}^3 \text{ g}^{-1}$ and $256.80 \text{ m}^2 \text{ g}^{-1}$, respectively, which are much larger than those of pure LDH ($0.25 \text{ cm}^3 \text{ g}^{-1}$ and $85.01 \text{ m}^2 \text{ g}^{-1}$, respectively). It has been proven that the addition of GO and an in situ growth process can decrease the aggregation of NiAl-LDH, resulting in more exposed LDH nanosheets and an enlarged specific surface area [30]. Fig. 4B displays the pore size distribution curves of LDH and rGO/LDH, for which the size distribution of rGO/LDH and pure LDH are 4.52 nm and 4.53 nm, respectively.

Fig. 5 displays the FT-IR spectra of GO and rGO/LDH. In the spectrum of rGO/LDH, we observe that the stretching vibrations of C–O (carboxylic acid) at 1870 cm^{-1} and C–O–H (alkoxy) at 1086 cm^{-1} have almost disappeared compared with pure GO, suggesting an effective reduction of GO to rGO. Furthermore, a peak at

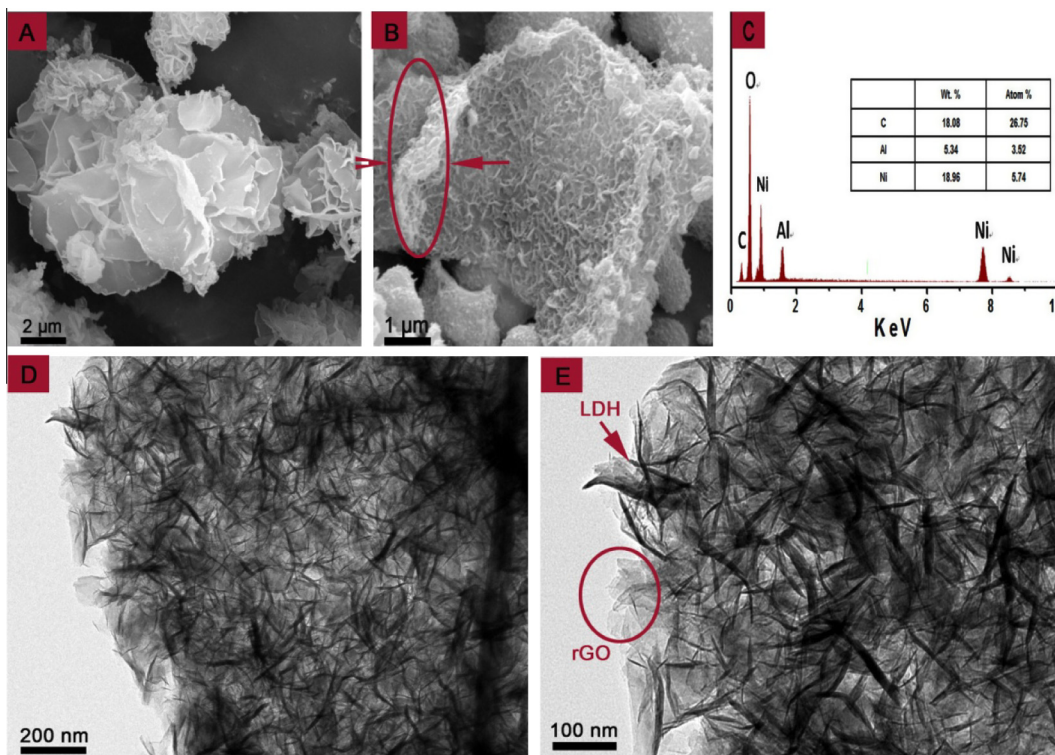


Fig. 3. SEM images of pure LDH (A), the rGO/LDH composite (B), the EDS spectrum of the rGO/LDH composite (C), TEM images at different magnifications of the rGO/LDH composite (D and E).

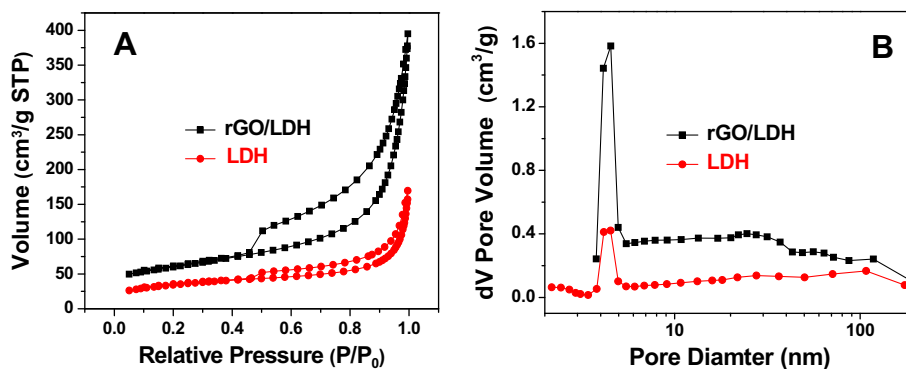


Fig. 4. The N₂ adsorption/desorption isotherms (A) and pore size distributions of rGO/LDH and LDH (B).

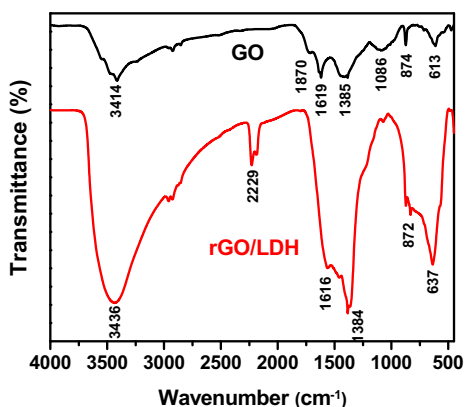


Fig. 5. FT-IR spectra of GO and rGO/LDH.

3436 cm⁻¹ is assigned to O–H, and the stretching vibrations at 1384 and 872 cm⁻¹, which are associated with CO₃²⁻ in the composite markedly increase, showing that carbonate ions and water molecules have been successfully intercalated into the interlayer spaces of NiAl–LDH during the assembly process [30]. At the same time, some of the bands below 800 cm⁻¹ are ascribed to the characteristic bending vibrations of metal–oxygen (M–O) bond [30,36], demonstrating the existence of NiAl–LDH in the composite.

3.2. Effect of initial pH

The solution pH is one of the most important factors controlling the metal ion adsorption process. The adsorption of uranium (VI) onto rGO/LDH was carried out by varying pH in the range of 2.00–12.00, and the results display a strong dependence of sorption on solution pH (Fig. 6). The amount of uranium (VI) adsorbed

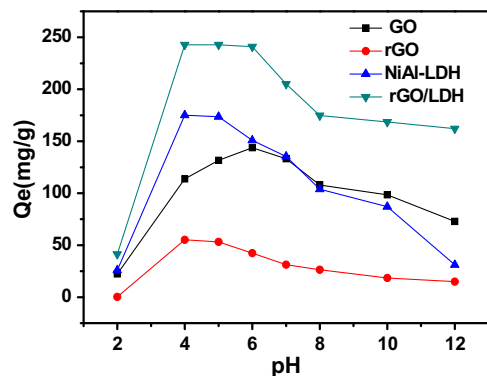


Fig. 6. Effect of initial pH on adsorption property of GO, rGO, NiAl-LDH, and rGO/LDH. pH = 2.00–12.00; $T = 25\text{ }^{\circ}\text{C}$; amount of adsorbent 0.01 g; Initial uranium concentration 120 mg L^{-1} .

on rGO/LDH increases greatly from 2.00 to 4.00, then changes little at pH 4.00–6.00, and the decrease is not significant from 6.00 to 12.00.

At $\text{pH} \leq 4.00$, uranium (VI) is present in solution predominantly in the form of UO_2^{2+} and the sorption is low because of the competition of H^+ ions for the binding sites of the adsorbents [37]. At pH 4.00–8.00, hydrolysis of uranyl ions occurs to produce products that include $\text{UO}_2(\text{OH})^+$, $(\text{UO}_2)(\text{OH})_2$, $(\text{UO}_2)_3(\text{OH})_5^+$ and $(\text{UO}_2)_2(\text{OH})_2^{2+}$, which are available for uranium (VI) adsorption on rGO/LDH [38], the sorption reaches a maximum. When the pH values rise to more than 8.00, the $(\text{UO}_2)_3(\text{OH})_7^-$ anions increases; these anions are known for their low sorption affinity, so the amount of uranium (VI) uptake decreases. As a consequence, the pH of solution equilibrium at 4.00 is the optimum for the adsorption of uranium (VI) on rGO/LDH.

The adsorption of uranium (VI) onto GO, rGO, NiAl-LDH, and rGO/LDH was carried out by varying pH in the range of 2.00–12.00 (Fig. 6). rGO shows low adsorption capacity for uranium, indicating that rGO has a rare contribution for uranium removal in the composite. In contrast, NiAl-LDH, and rGO/LDH have high adsorption capacity for uranium, meaning that NiAl-LDH mostly contribute to uranium removal in the composite. rGO/LDH shows high adsorption capacity for uranium, indicating this uniquely structured composite are favorable for achieving high adsorption performance.

3.3. Effect of adsorbent dose

The adsorbent dose is a key influence factor for the adsorption equilibrium. To examine the effect of adsorbent dose on the uranium (VI) removal, adsorption experiments were set up with various amounts of rGO/LDH from 0.005 to 0.1 g. Fig. 7 shows the effect of adsorbent dose on the removal efficiency, adsorption capacity, and the theoretical maximum adsorption capacity of uranium (VI). We observe that the removal efficiency of uranium (VI) increases rapidly with increasing dosage of rGO/LDH and then approaches equilibrium, while the adsorption capacity decreases. This is due to enhanced number of active sites with an increase in rGO/LDH. The percentage of uranium removal approaches equilibrium ($\geq 99\%$) at a dosage of rGO/LDH 0.01 g. Taking into account the removal efficiency and economical aspect, an adsorption dosage of 0.01 g was selected for the following studies.

3.4. Effect of contact time and adsorption dynamics

To determine the equilibrium time for maximum uptake and to establish the kinetics of adsorption process, uranium adsorption on

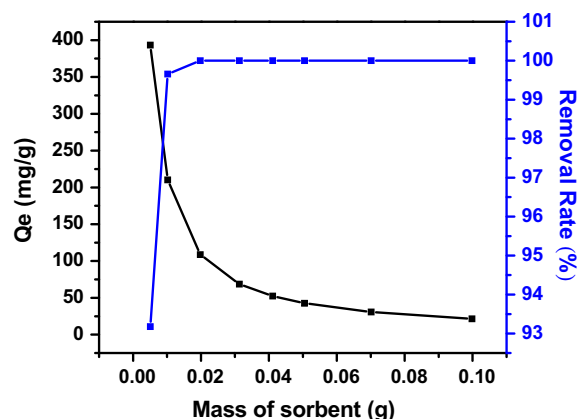


Fig. 7. The effect of adsorbent dose on the uptake of uranium (VI) by rGO/LDH. pH 4.00; temperature $25\text{ }^{\circ}\text{C}$; amount of rGO/LDH 0.005–0.10 g; initial uranium concentration 130 mg L^{-1} .

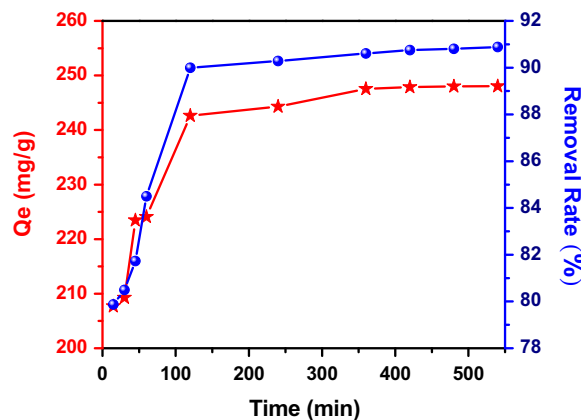


Fig. 8. Effect of contact time on uranium (VI) adsorption. pH 4.00; temperature $25\text{ }^{\circ}\text{C}$; amount of rGO/LDH 0.01 g; initial uranium concentration 130 mg L^{-1} .

rGO/LDH was examined as a function of contact time, as seen from Fig. 8. The maximum amounts of adsorption of uranium (VI) on rGO/LDH are observed at about 120 min. There is almost no further increase of adsorption after 120 min.

To evaluate the adsorption kinetics of uranium (VI) ions, pseudo-first-order and pseudo-second-order models were applied to analyze the experimental data [39–41]. The pseudo-first-order kinetic equation is given as

$$\ln(q_e - q_t) = \ln q_e - k_1 t \quad (3)$$

where k_1 is the rate constant of pseudo-first-order adsorption, q_e and q_t (mg g^{-1}) is the amount of uranium adsorbed at equilibrium and at time (t), respectively.

The values of q_e and k_1 are calculated from the intercepts and slopes of the plot (Fig. 9A) corresponding to Eq. (3), which are given in Table 1. The low-related coefficient R and the large difference between the calculated values of adsorption capacity and the experimental values indicate that the sorption mechanism of uranium (VI) on rGO/LDH does not follow a pseudo-first-order kinetic model well.

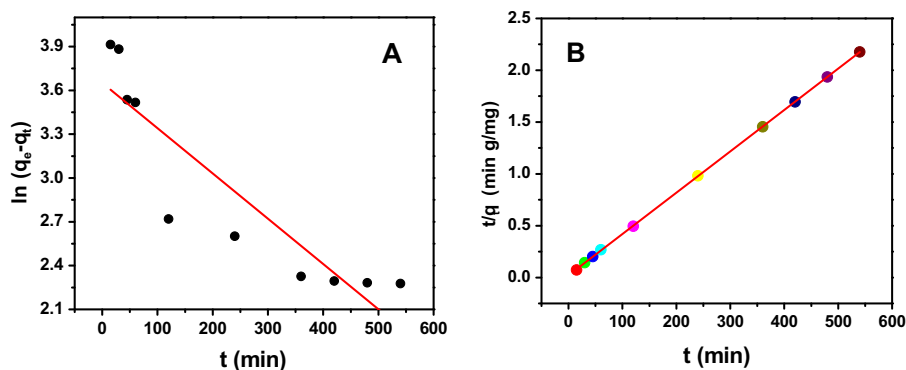
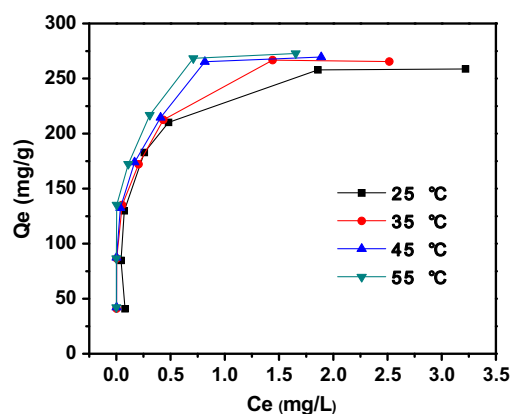
The pseudo-second-order adsorption kinetic model is defined as

$$t/q_t = 1/k_2 \cdot q_e^2 + t/q_e \quad (4)$$

where k_2 is the rate constant of pseudo-second-order adsorption. Fig. 9B shows straight lines of the pseudo-second-order model with

Table 1Pseudo-first-order and pseudo-second-order constants and values of R^2 for rGO/LDH.

Kinetic model	T (°C)	C_0 (mg/L)	Q_e^{exp} (mg/g)	Q_e^{cal} (mg/g)	$k_1(\text{min}^{-1})/k_2$ (g/mg min)	R^2
Pseudo-first order	25	130	257.8	38.55	0.0031	0.8031
Pseudo-second order	25	130	257.8	250.6	7.73×10^{-4}	0.9999

**Fig. 9.** Pseudo-first-order (A), pseudo-second-order (B), plot for the removal of uranium (VI) by rGO/LDH. pH 4.00; temperature 25 °C; amount of rGO/LDH 0.01 g.**Fig. 10.** Adsorption isotherm of rGO/LDH for uranium (VI) at different temperatures. pH 4.00; temperature 25–55 °C; amount of rGO/LDH 0.01 g; initial uranium concentration 20–130 mg L⁻¹.

correlation coefficients of 0.9999. Therefore, the adsorption kinetic fits the pseudo-second-order model.

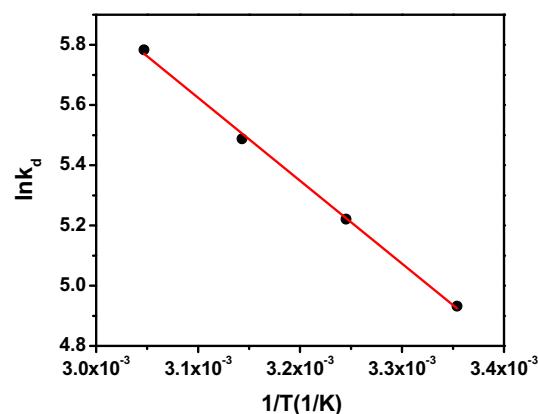
3.5. Effect of temperature and adsorption thermodynamics

To evaluate the influence of temperature on the adsorption process of uranium (VI) onto rGO/LDH, thermodynamic parameters were calculated at various temperatures. The sorption capacities as a function of temperature are plotted in Fig. 10, which show that the uptake of uranium (VI) increases with increasing temperature, indicating the endothermic nature of the process.

The temperature dependence of adsorption process is associated with changes in several thermodynamic parameters such as standard free energy (ΔG°), enthalpy (ΔH°) and entropy (ΔS°) of adsorption, which are calculated using the Van't Hoff equation shown in Eq. (5):

$$\ln K_d = -\Delta H^\circ / RT + \Delta S^\circ / R \quad (5)$$

where K_d is the distribution coefficient (mL g⁻¹), ΔH° is standard enthalpy (kJ mol⁻¹), ΔS° is standard entropy (J mol⁻¹ K⁻¹), T is the absolute temperature (K), and R is the gas constant (8.314 J mol⁻¹ K⁻¹).

**Fig. 11.** Relationship curve between $\ln K_d$ and $1/T$.

The values of ΔH° and ΔS° are evaluated from the intercept and slope of the linear plot of $\ln K_d$ vs. $1/T$ (Fig. 11). The positive value of ΔH° indicates the endothermic nature adsorption process. The positive standard entropy (ΔS°) indicates the increased randomness at the solid/liquid interface during the adsorption of uranium (VI) on rGO/LDH.

The standard free energy values were calculated from:

$$\Delta G^\circ = \Delta H^\circ - T \cdot \Delta S^\circ \quad (6)$$

where ΔG° is the standard Gibbs free energy. From Eq. (6), the data of ΔG° at different temperatures are obtained. The data of ΔG° , ΔH° and ΔS° are shown in Table 2. The Gibbs free energy decreases with increase in temperature, which suggests the feasibility and spontaneity of the adsorption process.

3.6. Adsorption isotherms of uranium

The equilibrium data were analyzed with the help of Langmuir isotherm and Freundlich isotherm models to obtain the best fitting isotherm. These two models are the most common isotherms used to describe the solid–liquid adsorption system.

Table 2
Thermodynamics parameters for uranium adsorption on rGO/LDH.

ΔH° (kJ mol ⁻¹)	ΔS° (J mol ⁻¹ K ⁻¹)	ΔG° (kJ mol ⁻¹)			
22.90	117.71	298 K –12.08	308 K –13.35	318 K –14.53	328 K –15.71

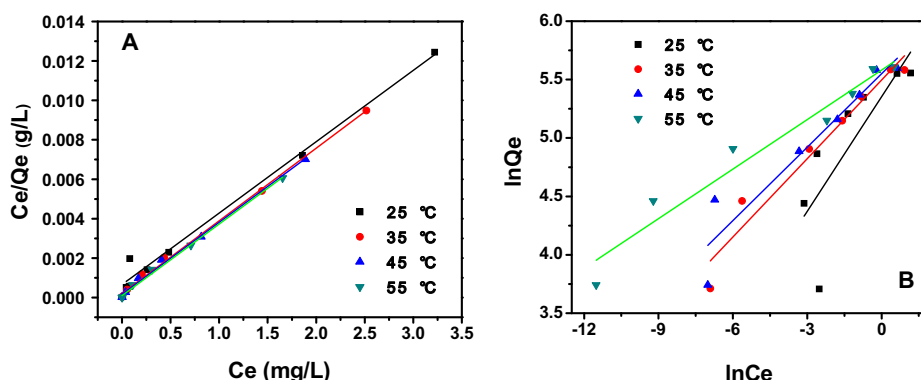


Fig. 12. Langmuir (A) and Freundlich (B) plots for the removal of uranium (VI) by rGO/LDH. pH 4.00; temperature 25–55 °C; amount of rGO/LDH 0.01 g.

Table 3
Isotherm constants and values of R^2 for rGO/LDH.

T (K)	Langmuir isotherm			Freundlich isotherm		
	Q_m (mg g ⁻¹)	b (L mg ⁻¹)	R^2	K (L g ⁻¹)	n	R^2
298	277.8	5.441	0.9862	211.2	3.063	0.5678
308	270.3	18.14	0.9976	243.7	4.461	0.9447
318	277.8	21.69	0.9952	257.2	4.771	0.8951
328	277.8	36.81	0.9963	265.6	7.067	0.9441

The Langmuir equation has been used extensively for dilute solutions in the following form [42]:

$$C_e/q_e = 1/b \cdot q_m + C_e/q_m \quad (7)$$

where C_e (mg L⁻¹) is the solute equilibrium concentration, q_e (mg g⁻¹) is the amount of solution adsorbed per unit mass of the adsorbent, q_m is the maximum adsorption capacity (mg g⁻¹), b is Langmuir constant. According to Eq. (7), a straight line is obtained and presented in Fig. 12A. The values of q_m and b are calculated from the slope and the intercept, and are given in Table 3.

The efficiency of the adsorption is expressed in terms of a dimensionless constant separation factor or equilibrium parameter R_L , which is defined as follows [43]:

$$R_L = 1/(1 + bC_0) \quad (8)$$

where C_0 is the initial metal ion concentration. The values of R_L show the isotherm shapes, which are unfavorable ($R_L \geq 1$) or favorable ($0 \leq R_L \leq 1$).

In this study R_L value as 0.0021 indicates that rGO/LDH is a suitable adsorbent for adsorption of uranium (VI) from aqueous solutions.

The Freundlich isotherm can be applied for heterogeneous surfaces and multilayer adsorption, which is expressed as follows [44]:

$$\ln q_e = \ln k + \frac{1}{n} \ln C_e \quad (9)$$

where k and n are the Freundlich constants related to the adsorption capacity and adsorption intensity, respectively. They are deter-

mined from the intercept and slope of the linear plot of $\ln q_e$ vs. $\ln C_e$ (Fig. 12B).

Table 3 shows that the Langmuir isotherm model better fits the experimental results over the experimental range, with high correlation coefficients (>0.99).

3.7. Test with simulated nuclear pollution seawater

To remove uranium from simulated nuclear pollution seawater, we prepared artificial seawater according to the composition reported in the literature [45]. Different concentrations of uranium (VI) were added to artificial seawater to prepare nuclear pollution seawater. The results are shown in Fig. 13. Due to the existence of a large number of other ions, the adsorption capacity of rGO/LDH from wastewater samples decreases. The concentration of other ions was thousands of times more than that of uranium (VI). The numbers of co-existing ions bring about a higher shielding effect for uranium (VI) ions at the rGO/LDH surface resulting in a reduction in sorption.

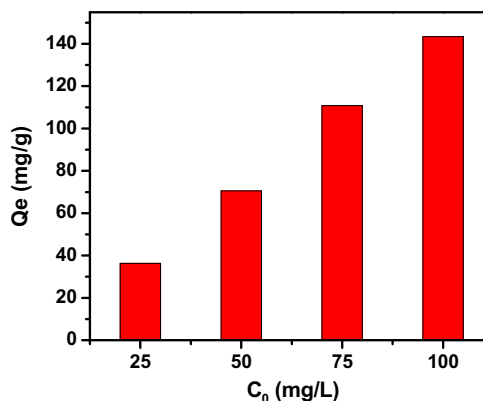


Fig. 13. Adsorption capacity of uranium (VI) from simulated nuclear pollution seawater sample with different concentrations of uranium (VI) (25, 50, 75, 100 mg L⁻¹) by rGO/LDH.

Table 4

Comparison of the uranium (VI) sorption capacity of rGO/LDH with other sorbents.

Sorbents	Experimental conditions	Q_{max} (mg g ⁻¹)	Refs.
Graphene oxide nanosheets	$T = 293$ K, pH = 5.0	97.5	[46]
Fe ₃ O ₄ /graphene oxide	$T = 293$ K, pH = 5.5	69.5	[47]
Functionalized polymer-coated silica	$T = 293$ K, pH = 5.0	5.2	[48]
Amine modified silica gel	$T = 302$ K, pH = 4.0	21.4	[49]
Amidoxime modified Fe ₃ O ₄ @SiO ₂	$T = 298$ K, pH = 5.0	105.5	[50]
Oxime-grafted CMK-5	$T = 298$ K, pH = 4.0	62	[51]
rGO/LDH	$T = 298$ K, pH = 4.0	277.8	Present work

Table 5

Desorption yields of some desorptive solutions.

	Desorption solvent	Concentration (mol L ⁻¹)	Desorption efficiency (%)
1	H ₂ O		6.35
2	Na ₂ EDTA	0.1	62.54
3	NaOH	0.1	45.89
4	Na ₂ SO ₄	0.1	2.72
5	Na ₂ CO ₃	0.1	69.59
6	NaHCO ₃	0.1	88.68

3.8. Comparison of adsorbent performance with literature data

A comparison of q_{max} values for uranium (VI) on rGO/LDH with those reported previously using different adsorbents is shown in Table 4. The maximum adsorption capacity of rGO/LDH is excellent compared to other adsorbents. The uranium (VI) removal capacities of other adsorbents, such as graphene oxide nanosheets, Fe₃O₄/graphene oxide, functionalized polymer-coated silica, amidoxime modified Fe₃O₄@SiO₂ are lower than that of rGO/LDH [46–48,50]. Thus, the comparison suggests that rGO/LDH have great potential as heavy metal ion adsorbents in wastewater treatment.

3.9. Removal mechanism

The adsorption capacity of rGO/LDH for uranium (VI) is 277.80 mg g⁻¹ in this study, which is higher than most of the previously reported values of other materials. This can be attributed to two reasons: first, the presence of functional groups (such as C–H, –OH, and –COOH) on the surface of rGO assures the capture of metallic cations (UO²⁺) by surface complexation mechanisms. Second, for the reaction of LDH with different pollutions, there are three possible reaction mechanisms [52]: The layered cation-exchange mechanism; the interlayer anion-exchange mechanism; the surface adsorption or complexation mechanism. Traditionally, the interlayer anion-exchange mechanism and the layered cation-exchange mechanism were acted on anionic pollutants and metal ions, respectively. Obviously, both of them can not used as mechanism for uranium removal because of uranyl is present in the majority of known uranium (VI) forms. Consequently, adsorption of uranium (VI) on the surface of LDH support may depends on complexation. Based on the above discussions, it was indicated that the surface adsorption or complexation mechanism act on rGO/LDH in the adsorption process of uranium. Further studies are needed to more precisely characterize the detailed adsorption mechanism.

3.10. Desorption and reusability study

Reusability is an important process in sorption studies due to it enhancing efficiency of use. Therefore, the reusability of rGO/LDH was investigated to evaluate its application potential in removal and recovery of uranium (VI). As illustrated in Table 5, the rGO/

LDH shows a lower desorption yield using NaOH, Na₂SO₄, and H₂O compared to other desorptive solutions. 0.1 mol L⁻¹ NaHCO₃ (88.68%) represents a high desorption yield for uranium. Hence, desorption tests showed that uranium is quantitatively desorbed with NaHCO₃.

To evaluate the regeneration of the adsorbent, the adsorption/desorption cycle was repeated three times with the same adsorbent using 0.1 mol L⁻¹ NaHCO₃ as desorbing agent. After three cycles, the sorption capacity of the rGO/LDH decreases from 252.81 mg g⁻¹ to 245.62 mg g⁻¹. This result shows that the adsorbent can be used efficiently in a real process such as nuclear industry wastewater treatment.

4. Conclusions

In conclusion, an interesting sandwich structure of rGO/NiAl–LDH composite has been fabricated, with its structure well-characterized by XRD, FT-IR, TEM and BET. The results show that NiAl–LDH nanosheet arrays grow perpendicularly and uniformly on both sides of the graphene sheets, constructing a hierarchical 3D nanocomposite with a sandwich structure. This composite has a large specific surface area and typical mesoporous characteristics. Compared to previous studies, rGO/LDH composite exhibits higher adsorption capacity in removing uranium (VI) from aqueous solution. The maximum sorption capacity of the rGO/LDH composite for uranium (VI) was evaluated to be 277.80 mg g⁻¹ at pH 4.00. The adsorption is highly dependent on the pH value. The adsorption followed pseudo-second-order kinetics and the equilibrium data were well fitted with Langmuir isotherms. Thermodynamic data suggest that the sorption of uranium (VI) on rGO/LDH is a spontaneous and endothermic process. The rGO/LDH as a novel adsorbent exhibits a bright future for practical applications in uranium (VI) from aqueous solutions.

Acknowledgment

This work was supported by National Natural Science Foundation of China (21353003), Special Innovation Talents of Harbin Science and Technology (2013RFQXJ145), Fundamental Research Funds of the Central University (HEUCFZ), Natural Science Foundation of Heilongjiang Province (B201316), Program of International S&T Cooperation special project (2013DFA50480), and the fund for Transformation of Scientific and Technological Achievements of Harbin (2013DB4BG011), Research and Development of Industrial Technology Project of Jilin Province (JF2012C022-4).

References

- [1] World Energy Perspective: Nuclear Energy One Year After Fukushima, World Energy Council, London, 2012.
- [2] A.M. Omer, *Energy, environment and sustainable development, Renew. Sustain. Energy Rev.* 12 (2008) 2265–2300.
- [3] H. Maeda, The global nuclear fuel market: supply and demand, in: Proceedings of The World Nuclear Association Annual Symposium, London, 2005, pp 2005–2030.

- [4] J. Schaller, A. Weiske, E.G. Dudel, Effects of gamma-sterilization on DOC, uranium and arsenic remobilization from organic and microbial rich stream sediments, *Sci. Total Environ.* 409 (2011) 3211–3214.
- [5] C.K. Gupta, H. Singh, *Uranium Resource Processing: Secondary Resources*, Springer-Verlag, Berlin, 2003.
- [6] J.C.B.S. Amaral, C.A. Morais, Thorium and uranium extraction from rare earth elements in monazite sulfuric acid liquor through solvent extraction, *Miner. Eng.* 23 (2010) 498–503.
- [7] P. Thakur, P. Chakravorty, K.C. Dash, T.R. Ramamohan, M.L.P. Reddy, Synergistic extraction of uranium(VI) by mixtures of beta-diketones and structurally related crown ethers, *Radiochim. Acta* 80 (1998) 155–161.
- [8] A.M.S. John, R.W. Cattrall, S.D. Kolev, Extraction of uranium(VI) from sulfate solutions using a polymer inclusion membrane containing di-(2-ethylhexyl) phosphoric acid, *J. Membr. Biol.* 364 (2010) 354–361.
- [9] C.A. Morais, L.A. Gomiero, Uranium stripping from tertiary amine loaded solution by ammonium sulfate, *Miner. Eng.* 18 (2005) 1277–1281.
- [10] M. Owlad, M.K. Aroua, W.A.W. Daud, S. Baroutian, Removal of hexavalent chromium-contaminated water and wastewater: a review, *Water Air Soil Pollut.* 200 (2009) 59–77.
- [11] S.E. Bailey, T.J. Olin, R.M. Brika, D.D. Adrian, A review of potentially low-cost sorbents for heavy metals, *Water Res.* 33 (1999) 2469–2479.
- [12] P. Miretzky, A.F. Cirelli, Cr (VI) and Cr (III) removal from aqueous solution by raw and modified lignocellulosic materials: a review, *J. Hazard. Mater.* 180 (2010) 1–19.
- [13] M. Lehmann, A.I. Zouboulis, K.A. Matis, Removal of metal ions from dilute aqueous solutions: a comparative study of inorganic sorbent materials, *Chemosphere* 39 (1999) 881–892.
- [14] Q. Su, S. Pang, V. Alijani, C. Li, X. Feng, K. Mullen, Composites of graphene with large aromatic molecules, *Adv. Mater.* 21 (2009) 3191–3195.
- [15] K. Loh, Q. Bao, P.K. Ang, J. Yang, The chemistry of graphene, *J. Mater. Chem.* 20 (2010) 2277–2289.
- [16] K. Lü, G. Zhao, X. Wang, A brief review of graphene-based material synthesis and its application in environmental pollution management, *Chin. Sci. Bull.* 57 (2012) 1223–1234.
- [17] R. Zacharia, H. Ulbricht, T. Hertel, Interlayer cohesive energy of graphite from thermal desorption of polyaromatic hydrocarbons, *Phys. Rev. B* 69 (2004) 155406.
- [18] Z. Wu, D. Wang, W. Ren, J. Zhao, G. Zhou, F. Li, H. Cheng, Anchoring hydrous RuO₂ on graphene sheets for high-performance electrochemical capacitors, *Adv. Funct. Mater.* 20 (2010) 3595–3602.
- [19] L. Peng, X. Peng, B. Liu, C. Wu, Y. Xie, G. Yu, Ultrathin two-dimensional MnO₂/graphene hybrid nanostructures for high-performance, flexible planar supercapacitors, *Nano Lett.* 13 (2013) 2151.
- [20] X. Huang, Z. Zeng, Z. Fan, J. Liu, H. Zhang, Graphene-based electrodes, *Adv. Mater.* 24 (2012) 5979.
- [21] H. Wang, H.S. Casalongue, Y. Liang, H. Dai, Ni(OH)₂ nanoplates grown on graphene as advanced electrochemical pseudocapacitor materials, *J. Am. Chem. Soc.* 132 (2010) 7472.
- [22] Z. Liu, R. Ma, M. Osada, N. Iyi, Y. Ebina, K. Takada, T. Sasaki, Synthesis, anion exchange, and delamination of co–al layered double hydroxide: assembly of the exfoliated nanosheet/polyanion composite films and magneto-optical studies, *J. Am. Chem. Soc.* 128 (2006) 4872.
- [23] Y. Guo, Z. Zhu, Y. Qiu, J. Zhao, Enhanced adsorption of acid brown 14 dye on calcined Mg/Fe layered double hydroxide with memory effect, *Chem. Eng. J.* 219 (2013) 69.
- [24] A. Garcia-Gallastegui, D. Iruretagoyena, V. Gouvea, M. Mokhtar, A.M. Asiri, S.N. Basahel, S.A. Al-Thabaiti, A.O. Alyoubi, D. Chadwick, M.S.P. Shaffer, *Chem. Mater.* 24 (2012) 4531.
- [25] J. Han, Y. Dou, M. Wei, D.G. Evans, X. Duan, Erasable nanoporous antireflection coatings based on the reconstruction effect of layered double hydroxides, *Angew. Chem. Int. Ed.* 49 (2010) 2171.
- [26] J.L. Gunjekar, I.Y. Kim, J.M. Lee, N.-S. Lee, S.-J. Hwang, Self-assembly of layered double hydroxide 2D nanoplates with graphene nanosheets: an effective way to improve the photocatalytic activity of 2D nanostructured materials for visible light-induced O₂ generation, *Energy Environ. Sci.* 6 (2013) 1008.
- [27] W.S. Hummers, R.E. Offeman, Preparation of graphitic oxide, *J. Am. Chem. Soc.* 80 (1958) 1339.
- [28] Y. Zhao, S. He, M. Wei, D.G. Evans, X. Duan, Hierarchical films of layered double hydroxides by using a sol-gel process and their high adaptability in water treatment, *Chem. Commun.* (2010) 3031.
- [29] Z.H. Liu, Z.M. Wang, X. Yang, K. Ooi, Intercalation of organic ammonium ions into layered graphite oxide, *Langmuir* 18 (2002) 4926.
- [30] J. Fang, M. Li, Q. Li, W. Zhang, Q. Shou, F. Liu, X. Zhang, J. Cheng, Microwave-assisted synthesis of CoAl-layered double hydroxide/graphene oxide composite and its application in supercapacitors, *Electrochim. Acta* 85 (2012) 248.
- [31] M. Li, J.E. Zhu, L. Zhang, X. Chen, H. Zhang, F. Zhang, S. Xu, D.G. Evans, Facile synthesis of NiAl-layered double hydroxide/graphene hybrid with enhanced electrochemical properties for detection of dopamine, *Nanoscale* 3 (2011) 4240.
- [32] H. Wang, X. Xiang, F. Li, Facile synthesis and novel electrocatalytic performance of nanostructured Ni–Al layered double hydroxide/carbon nanotube composites, *Mater. Chem.* 20 (2010) 3944.
- [33] C. Nethravathi, T. Nisha, N. Ravishankar, C. Shivakumara, M. Rajamathi, Graphene–nanocrystalline metal sulphide composites produced by a one-pot reaction starting from graphite oxide, *Carbon* 47 (2009) 2054.
- [34] T.N. Lambert, C.A. Chavez, B. Hernandez-Sanchez, P. Lu, N.S. Bell, A. Ambrosini, T. Friedman, T.J. Boyle, D.R. Wheeler, D.L. Huber, Synthesis and characterization of titania–graphene nanocomposites, *J. Phys. Chem. C* 113 (2009) 19812.
- [35] C. Xu, X. Wu, J. Zhu, X. Wang, Synthesis of amphiphilic graphite oxide, *Carbon* 46 (2008) 386.
- [36] L. Zhang, X. Zhang, L. Shen, B. Gao, L. Hao, X. Lu, F. Zhang, B. Ding, C. Yuan, Enhanced high-current capacitive behavior of graphene/CoAl-layered double hydroxide composites as electrode material for supercapacitors, *J. Power Sources* 199 (2012) 395.
- [37] A. Schierz, H. Zaker, Aqueous suspensions of carbon nanotubes: surface oxidation, colloidal stability and uranium sorption, *Environ. Pollut.* 157 (2009) 1088–1094.
- [38] G. Wang, J. Liu, X. Wang, Z. Xie, N. Deng, Adsorption of uranium (VI) from aqueous solution onto cross-linked chitosan, *J. Hazard. Mater.* 168 (2009) 1053–1058.
- [39] Y.S. Ho, G. McKay, The kinetics of sorption of divalent metal ions onto sphagnum moss peat, *Water Res.* 34 (2000) 735.
- [40] J. Yu, H.B. Bai, J. Wang, Z.S. Li, C.S. Jiao, Q. Liu, M.L. Zhang, L.H. Liu, Synthesis of alumina nanosheets via supercritical fluid technology with high uranyl adsorptive capacity, *New J. Chem.* 37 (2013) 366.
- [41] Y. Miyake, H. Ishida, S. Tanaka, D. Kolev, S.D. Kolev, Theoretical analysis of the pseudo-second order kinetic model of adsorption. Application to the adsorption of Ag(I) to mesoporous silica microspheres functionalized with thiol groups, *Chem. Eng. J.* 218 (2013) 350.
- [42] I. Langmuir, The adsorption of gases on plane surfaces of glass mica and platinum, *J. Am. Chem. Soc.* 40 (1918) 1361–1403.
- [43] A. Bhatnagar, A.K. Jain, A comparative adsorption study with different industrial wastes as adsorbents for the removal of cationic dyes from water, *J. Colloid Interface Sci.* 28 (2005) 49–55.
- [44] Freundlich, Über die adsorption in losungen, *Z. Phys. Chem.* 57 (1906) 385–470.
- [45] Y. Gao, A. Mucci, Individual and competitive adsorption of phosphate and arsenate on goethite in artificial seawater, *Chem. Geol.* 199 (2003) 91–109.
- [46] G.X. Zhao, T. Wen, X. Yang, S.B. Yang, J.L. Liao, J. Hu, D.D. Shao, X.K. Wang, Preconcentration of U(VI) ions on few-layered graphene oxide nanosheets from aqueous solutions, *Dalton Trans.* 41 (2012) 6182–6188.
- [47] P.F. Zong, S.F. Wang, Y.L. Zhao, H. Wang, H. Pan, C.H. He, Synthesis and application of magnetic graphene/iron oxides composite for the removal of U (VI) from aqueous solutions, *Chem. Eng. J.* 220 (2013) 45–52.
- [48] D.E. Bryant, D.I. Stewart, T.P. Kee, C.S. Barton, Development of a functionalized polymer-coated silica for the removal of uranium from groundwater, *Environ. Sci. Technol.* 37 (2003) 4011–4016.
- [49] K.A. Venkatesan, V. Sukumaran, M.P. Antony, P.R.V. Rao, Extraction of uranium by amine, amide and benzamide grafted covalently on silica gel, *J. Radioanal. Nucl. Chem.* 260 (2004) 443–450.
- [50] Y.G. Zhao, J.X. Li, L.P. Zhao, S.W. Zhang, Y.S. Huang, X.L. Wu, X.K. Wang, Synthesis of amidoxime-functionalized Fe₃O₄/SiO₂ core-shell magnetic microspheres for highly efficient sorption of U(VI), *Chem. Eng. J.* 235 (2014) 275–283.
- [51] G. Tian, J.X. Geng, Y.D. Jin, C.L. Wang, S.Q. Li, Z. Chen, H. Wang, Y.S. Zhao, S.J. Li, Sorption of uranium(VI) using oxime-grafted ordered mesoporous carbon CMK-5, *J. Hazard. Mater.* 190 (2011) 442–450.
- [52] S.N. Li, H.B. Bai, J. Wang, X.Y. Jing, Q. Liu, M.L. Zhang, R.R. Chen, L.H. Liu, C.S. Jiao, In situ grown of nano-hydroxyapatite on magnetic CaAl-layered double hydroxides and its application in uranium removal, *Chem. Eng. J.* 193–194 (2012) 372–380.